Upscaling thermal conductivities of sedimentary formations for geothermal exploration

Wolfram Rühaak [a,e,*], Alberto Guadagnini [b,c], Sebastian Geiger [d], Kristian Bär [e], Yixi Gu [e], Achim Aretz [e], Sebastian Homuth [f], Ingo Sass [a,e]

[a] *Technische Universität Darmstadt, Darmstadt Graduate School of Excellence Energy Science and Engineering, Jovanka-Bontschits-Str. 2, 64287 Darmstadt, Germany*

[b] *Dipartimento di Ingegneria Civile e Ambientale, Politecnico di Milano, Piazza L. Da Vinci, 32, 20133 Milano, Italy*

[c] *Department of Hydrology and Water Resources, University of Arizona, Tucson, AZ 85721, USA*

[d] *Institute of Petroleum Engineering, Heriot-Watt University, Edinburgh, UK*

[e] *Technische Universität Darmstadt, Institute of Applied Geosciences, Department of Geothermal Science and Technology, Schnittspahnstr. 9, 64287 Darmstadt, Germany*

[f] *Züblin Spezialtiefbau GmbH Ground Engineering, Europa-Allee 50, 60327 Frankfurt a. M., Germany*

Received 8 November 2014
Received in revised form 16 July 2015
Accepted 13 August 2015

1. Introduction

Geothermal models for simulating heat and mass transfer are a key tool for geothermal exploration and planning (e.g. Rühaak et al., 2010; Sippel et al., 2013; Huenges et al., 2013). Inputs to such models include information/data on parameters such as permeability and thermal conductivity. Knowledge of the details of the spatial distribution of these system parameters is typically very limited. Measurements are associated with diverse sources and are distributed on a multiplicity of scales. These data can be obtained from different sources, including but not limited to well-logs, outcrop analogues, plugs, or thin sections (Fig. 1).

Remarkable databases of petrophysical properties in geothermal reservoirs have been maintained in the past (e.g. Sass et al., 1971; Haenel and Staroste, 1988; Williams and Anderson, 1990; Clauser and Huenges, 1995; Bär et al., 2011; Homuth et al., 2014).

Depending on the approach and data type availability, projecting these measurements onto reservoir models requires, for example, geostatistical/stochastic modeling, upscaling and possibly also downscaling. A key requirement associated with all these approaches is the intention to keep as much of the small scale information as possible while projecting their effect onto the model scale.

Several well-established modeling and upscaling techniques for petrophysical properties in hydrocarbon reservoirs can be found, a short review is added in this text. Few works exist about the upscaling of thermal conductivity for geothermal modeling (e.g. focusing

* Corresponding author at: Technische Universität Darmstadt, Institute of Applied Geosciences, Department of Geothermal Science and Technology, Schnittspahnstr. 9, 64287 Darmstadt, Germany.
E-mail address: ruehaak@geo.tu-darmstadt.de (W. Rühaak).

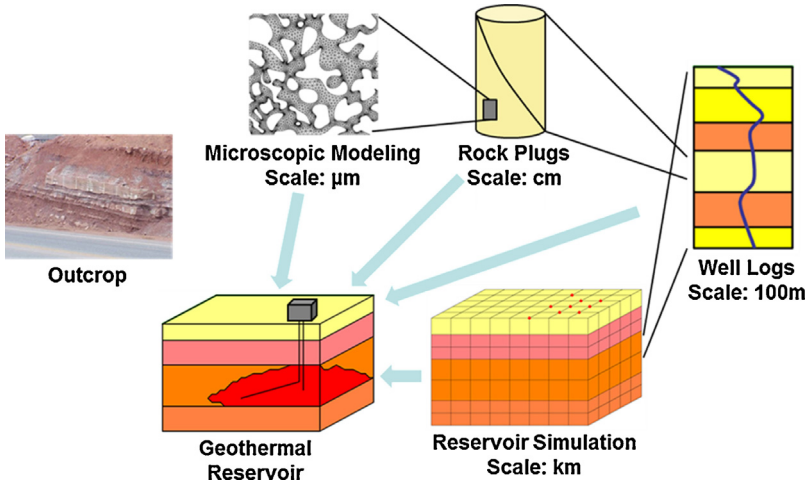

Fig. 1. The concept of upscaling from diverse scales to a desired model scale.

on crystalline rocks, Sundberg et al., 2009), but no established procedure exists.

Yet, geothermal reservoirs have a much tighter margin to be economically profitable. Therefore, being able to reliably model and upscale petrophysical properties in such reservoirs is of critical importance to reliably forecast heat in place and energy extraction.

There are diverse approaches to parameter upscaling. Numerical models with scales of several kilometers are discretized through a set of grid blocks; upscaling has to be performed for each grid block with typical sizes of tens to hundredth of meters. One approach is simply based on some type of averaging. However, the selection of the appropriate method of averaging (i.e., arithmetic, geometric, harmonic) depending on scale and flow conditions is not trivial and is a matter of the corresponding scale (Hartmann et al., 2005).

The following scales are typically defined and considered in numerical modeling and theoretical studies:

- Microscale (X-ray computer tomography, nuclear magnetic resonance (NMR), thin-sections, electron microscopy, mineralogy, fissures, microcracks).
- Mesoscale (rock-samples, cores, borehole-geophysics, NMR, positron emission tomography (PET), laboratory measurements of thermal conductivity, permeability, porosity, fractures, small scale modelling).
- Macroscale (seismics, gravimetry, magnetics, helicopter electromagnetics (HEM), fault zones, outcrop studies, remote sensing, medium–large scale modelling).

Following Scheibe and Yabusaki (1998) the aim of this work is to demonstrate the effects of thermal conductivity upscaling in general, rather than determining rules for upscaling and/or values of parameters for general use.

2. Upscaling of thermal and hydraulic conductivity

2.1. Constitutive relations

Several thermo-physical properties are relevant for assessing and planning geothermal exploration and production. Among these parameters, bulk permeability and thermal conductivity are critical for the assessment of the subsurface distribution of fluids and temperature field. A detailed analysis of the way upscaling strategies for thermal conductivity might impact temperature and pressure distributions and the assessment of the sustainability of a geothermal reservoir is still missing.

For example, Fig. 2 depicts the ranges of thermal conductivity values documented for diverse rock types and indicates the typical degree of spatial variability of this parameter.

Based on Fourier's law (Eq. (1)) the thermal conductivity λ (W m^{-1} K^{-1}) controls the rate of heat flow q (W m^{-2}) which results from a given temperature gradient ∇T (°C m^{-1}):

$$\mathbf{q} = -\boldsymbol{\lambda} \nabla T. \tag{1}$$

Heat transport equation in a geological formation occurs by a combination of convective and conductive processes. It is frequently modelled by the following equation (e.g. Nield and Bejan, 1999).

$$(\rho c)_g \frac{\partial T}{\partial t} = \nabla \cdot \left(\lambda_g \nabla T - (\rho c)_f \mathbf{v} T\right) + H \tag{2}$$

Here, T (°C) is temperature, c is specific heat capacity (J kg^{-1} K^{-1}), ρ is density (kg m^{-3}), λ is thermal conductivity (W m^{-1} K^{-1}), $\mathbf{v}$ is Darcy velocity (m s^{-1}), and H (W m^{-3}) represents sink/source terms. Subscripts f and g denote fluid and bulk properties, respectively.

Since heat transport in the subsurface is governed by the joint effects of conductive and convective processes, as seen in Eq. (2), a simple deduction of the thermal conductivity based on temperature or heat flow space–time distributions is fraught with theoretical and conceptual difficulties and can lead to ambiguous results.

As we are here interested in analyzing upscaling of thermal con-ductivity, λ, which is fundamentally different from upscaling of hydraulic conductivity as we illustrate in Section 2.2, we consider only pure conduction in Eq. (2) (i.e., when $\lambda_g \nabla T \gg (\rho c)_f \mathbf{v} T$). From a practical point of view, such situations can take place when the permeability of the host formation is approximately 10^{-15} m^2 or less (Hayba and Ingebritsen, 1997). Basin modelling studies often consider only conductive heat transport (e.g. Förster and Merriam, 1999; Beardsmore and Cull, 2001).

2.2. Key differences between upscaling of hydraulic and thermal conductivities

Upscaling of permeability and porosity has been the subject of several studies in the field of oil and gas exploration (Farmer, 2002) as well as in the groundwater hydrology literature.

Starting from the work of Clauser (1992) detailed reviews of the diverse upscaling techniques for hydraulic conductivity and permeability where provided, e.g. by Wen and Gomez-Hernandez (1996) and Renard and de Marsily (1997). Stochastic and deterministic

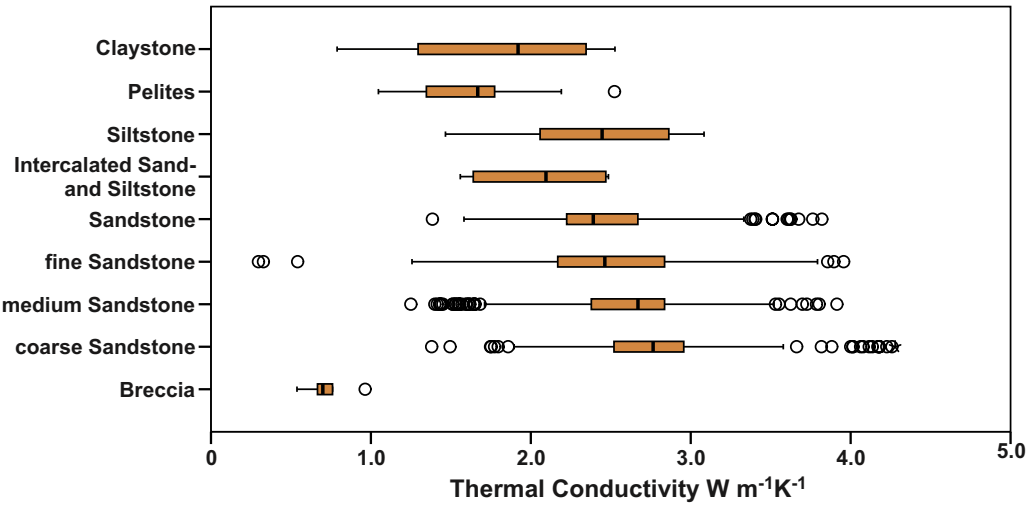

Fig. 2. Box–Whisker plots (after Tukey, 1977) of the thermal conductivity of different sedimentary rock types, illustrating the variability both in between different rock types as well as for one rock type. The Box is defined by the first and third quartile, the line inside the box is the median, the length of the whiskers is limited to 1.5 times of the distance between the quartiles, points indicate outliers, stars indicate outliers which are more than 3 times the distance between the quartiles.

upscaling approaches to asses representative values for hydraulic conductivities have been reviewed by Sánchez-Vila et al. (2006). Scaling of statistics of hydraulic conductivity and/or permeability, and other soil properties has been recently analyzed, amongst others by Neuman et al. (2013), Guadagnini et al. (2013, 2015) and references therein.

Upscaling of hydraulic and thermal conductivities share some similarities. Independent of the adopted theoretical approach, important differences can also be observed. These differences are related to the phenomenological basis according to which fluid flow and heat transport are described as well as to the diverse behavior of measured/estimated parameters. The range of documented hydraulic conductivity values of clastic sedimentary rocks (typically 10^{-3} m s^{-1}–10^{-12} m s^{-1}) is very dif-ferent from that associated with thermal conductivities (typically 0.5 W m^{-1} K^{-1}–4.5 W m^{-1} K^{-1}).

Sample probability distributions of hydraulic conductivity are often modeled as lognormal or through modern techniques based on the notion of sub-Gaussian processes (see, e.g. Riva et al., 2013; Guadagnini et al., 2015) while thermal conductivity is typically interpreted through Gaussian density models.

Another notable difference is that while fluid flow (as driven by hydraulic conductivity at a continuum scale) occurs only in the pore space, conductive temperature flux occurs within both the solid matrix and the pores. While hydraulic conductivity can be strongly anisotropic, thermal conductivity is generally observed to be isotropic.

2.3. Common upscaling techniques

Information included in data bases relevant for geothermal rock properties originate either from outcrops or from drillings. Transfer of these meso-scale information to the macro-scale (i.e., the numerical reservoir model) can be performed in principle through the following three approaches:

1 By lithological considerations: it is relatively well understood that (a) thermal conductivity of sedimentary rocks reflects the mineralogy, the cementation, the porosity and the compaction of the grains, while (b) thermal conductivity of volcanic/plutonic and metamorphic rocks reflects mainly the mineralogy (e.g. Clauser and Huenges, 1995). Additional factors that need to be considered include the reservoir conditions such as saturation degree, fluid type(s), temperature and pressure which can also strongly affect each lithological unit to different degrees. In this context, one can assume that by studying the broad geo-logical settings, in terms of spatial distribution of facies (Sass and Götz, 2012; Homuth et al., 2014), as well as commonali-ties between geological/mineralogical conditions may be used as basis to assign correspondingly similar thermal conductivity values.
2 By applying (geostatistical or deterministic) inter- and extrapolation techniques (Desbarats, 1992; Goovaerts, 1997; Chilès and Delfiner, 1999; Gu et al., 2013; Pyrcz and Deutsch, 2014).
3 By stochastic or deterministic inverse modelling (e.g. Rath et al., 2006; Vogt et al., 2010; Li et al., 2012), where observed values of thermal conductivity, q, and/or T (see Eq. (1)) can be used as a priori information.

Various studies have attempted to calculate the thermal conductivity based on the mineral content of rocks (e.g. Pribnow and Umsonst, 1993; Hartmann et al., 2005; Sundberg et al., 2009; Fuchs and Förster, 2010; Al-Zyoud et al., 2014). However the resulting values often show a strong bias when compared against measured bulk values and the applicability of this approach is limited if large scale values are required.

Based on differences which reflect the physical behaviour of rock types, it is unlikely that one can identify an upscaling procedure as universally valid for all types of rocks and environmental conditions. Instead, diverse procedures have to be considered depending on rock composition and (possibly) flow conditions.

Existing approaches to upscaling can loosely be grouped into either local (e.g. based on local averaging of the target property) vs. non-local methods (where the larger system is also considered in the upscaling procedure), or two-step vs. direct upscaling methods (Wen and Gomez-Hernandez, 1996).

Power averaging (Journel et al., 1986), as introduced in the con-text of hydraulic conductivity upscaling, is the most commonly applied upscaling technique. It can be expressed as (Scheibe and Yabusaki, 1998):

$$\bar{\lambda} = \left[\frac{1}{N} \sum_{i=1}^{N} \lambda_i^p \right]^{\frac{1}{p}} \tag{3}$$

where λ_i is the thermal conductivity of the ith element of the subdomain based on which upscaled conductivity values associated

with larger scales are estimated; N is the number of elements in the subdomain, and $\bar{\lambda}$ is the averaged (equivalent/representative) conductivity of the subdomain. The averaging exponent p is selected from the range $-1 <= p <= 1$ ($p \neq 0$). We note that $p = 1, -1$, respectively, define the arithmetic and the harmonic means. As $p = 0$ is invalid for averaging it is superseded by $p \to \infty$ which gives the geometric mean.

It is well known that the use of these means leads to upscaled properties related by

$$\text{harmonic mean} \leq \text{geometric mean} \leq \text{arithmetic mean} \tag{4}$$

Effective thermal conductivity of a layered system is equal to the volume averaged arithmetic or harmonic mean of the local conductivities, respectively for flow parallel or normal to the direction of layering (Hartmann et al., 2005). For the simple case of a two-layer system, this implies that:

$$\bar{\lambda}_a = V_1\lambda_1 + V_2\lambda_2 \tag{5}$$

$$\bar{\lambda}_h = \frac{V_1}{\lambda_1} + \frac{V_2}{\lambda_2} \tag{6}$$

where λ_1 and λ_2, respectively are the conductivities of medium 1 and 2, associated with volumetric proportions V_1 and V_2. Subscripts a and H denote arithmetic and harmonic averages, respectively.

Christie (2001) states that the most promising methods proposed in the last few years may be those that regard upscaling as an integral part of the solution of the flow equations, rather than as an external process which must be complemented with appropriate boundary conditions to provide an appropriate answer. This view is still not convincingly supported either by unambiguous and rigorous theoretical arguments or by results based on numerical simulations on synthetic or real life settings.

A comparison between flow based upscaling (so called pressure solver methods) against renormalization approaches is given by Christie (1996), while a comparison between inverse based upscaling and renormalization is given by Lunati et al. (2001).

In the context of heat flow, a flow based upscaling may be understood as an approach leading to integrated (or global) thermal conductivities. This can be expressed as the numerical solution for an effective volumetric thermal conductivity, by rearranging the classical Fourier Law as Eq. (1):

$$\int_V \lambda = \frac{q}{\nabla T} \tag{7}$$

q being the rate of heat flow q (W m^{-2}) which results from a given temperature gradient ∇T ($^\circ$C m^{-1}).

Renormalization was first introduced by King (1989) for upscaling of permeabilities. Following Hastings and Muggeridge (2001), the principle is to take a subregion formed by an array of two by two cells as the smallest unit and then employ an analogy with a cir-cuit of electrical resistors to calculate a representative/equivalent property. The general idea is illustrated in Fig. 3. The resulting (rep-resentative) value of the property is then used as one of the four cell properties at the following, larger, length scale, and so on. An advantage of this procedure is that calculating effective properties relies on an analytical expression and hence successive upscaling is straightforward.

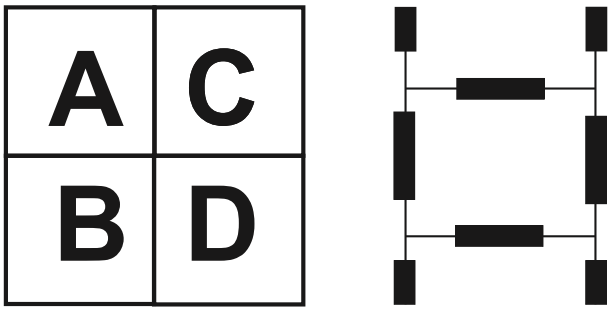

Fig. 3. Schematic of the resistor analogue used in small cell renormalization (Hastings and Muggeridge, 2001).

Fig. 4. Photograph of a Carboniferous to Permian Rotliegend sandstone outcrop (Oberkirch formation) close to the town of Hochstätten (50 km southwest of Frankfurt am Main, Germany) (a), a closer view on a stratigraphic section from the Messel borehole GA2 (b) and samples (c) taken at this outcrop showing the heterogeneities at different scales (a) meter to hundreds of meter scale, (b) decimeter to meter scale and (c) millimeter to centimeter scale.

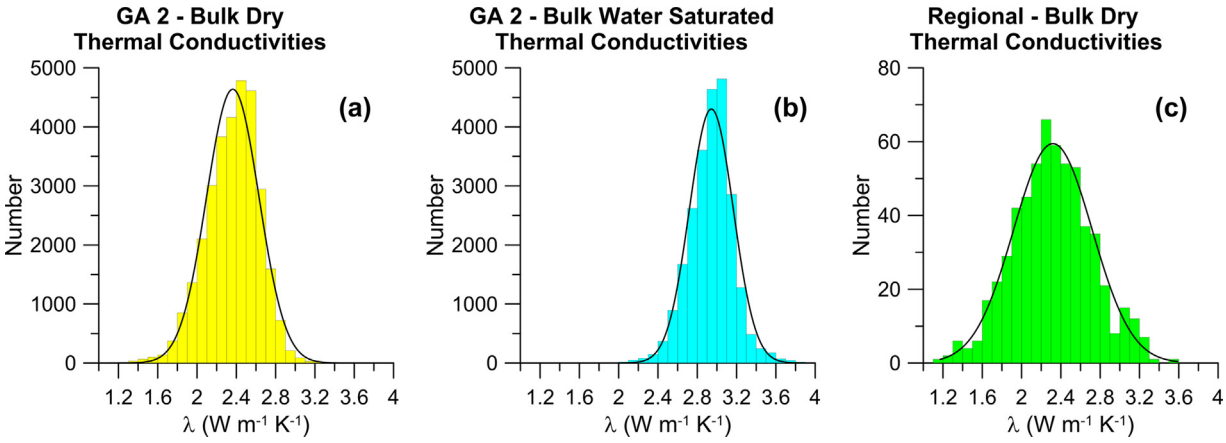

Fig. 5. Histograms for the (a) vertical dataset measured at dry conditions, (b) vertical dataset measured at water saturated conditions and (c) regional horizontal distribute dataset measured at dry conditions.

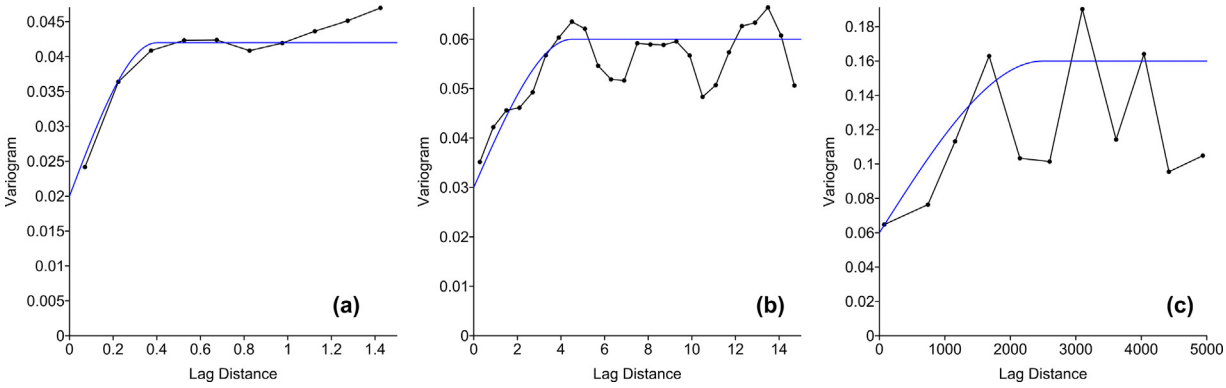

Fig. 6. Experimental and theoretical variograms (a) for the small (Table 2, vertical one-dimensional), (b) intermediate (Table 2, vertical one-dimensional) and (c) large scale (Table 4, horizontal two-dimensional omnidirectional) datasets, respectively. All variograms are based on dry measured values.

The analytical expression for block effective thermal conductivity $\lambda_{2\times2}$ using the resistor analogue is (Hastings and Muggeridge, 2001):

$$\lambda_{2\times2} = \frac{4(A+C)(B+D)[BD(A+C)+AC(B+D)]}{[BD(A+C)+AC(B+D)][A+B+C+D]+3(A+B)(C+D)(A+C)(B+D)} \quad (8)$$

where the same notation as provided in Fig. 3 is employed.

In comparison to a two-dimensional solution, it is remarked that a three-dimensional solution is far more complex to derive (Green and Paterson, 2007; Karim and Krabbenhoft, 2010).

Other upscaling approaches discussed in literature with reference to transfer of information between meso- to macro-scale continuum models, but not used in the study presented here, include:

- Wavelets (Press et al., 1992); this approach is for instance used in the field of image processing as it allows reflecting the main characteristics of a property distribution both on small and large scales. Application of wavelets to geoscientific upscaling has become very popular (Lu, 2001; Chu and Schatzinger, 1996; Reza Rasaei and Sahimi, 2008) since the early 1990.
- A combination of upscaling and inverse modeling using the Ensemble Kalman Filter (EnKF), as given, e.g. by Li et al. (2012).
- A multilevel upscaling approach using multigrid solvers and operator-induced variational coarsening, as suggested and analyzed by MacLachlan and Moulton (2006).
- Upscaling of shale rock properties based on three-dimensional imaging and modeling, as discussed by Zhang et al. (2012).

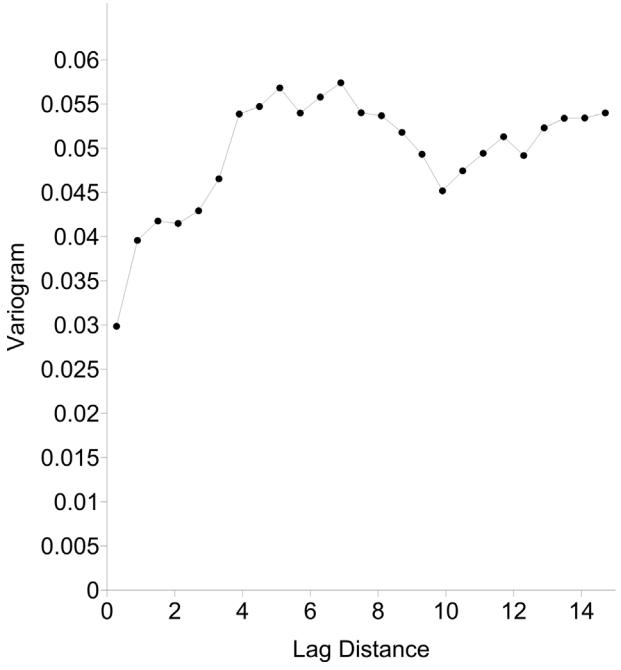

Fig. 7. Experimental variogram for the vertical one-dimensional dataset based on water saturated measurements.

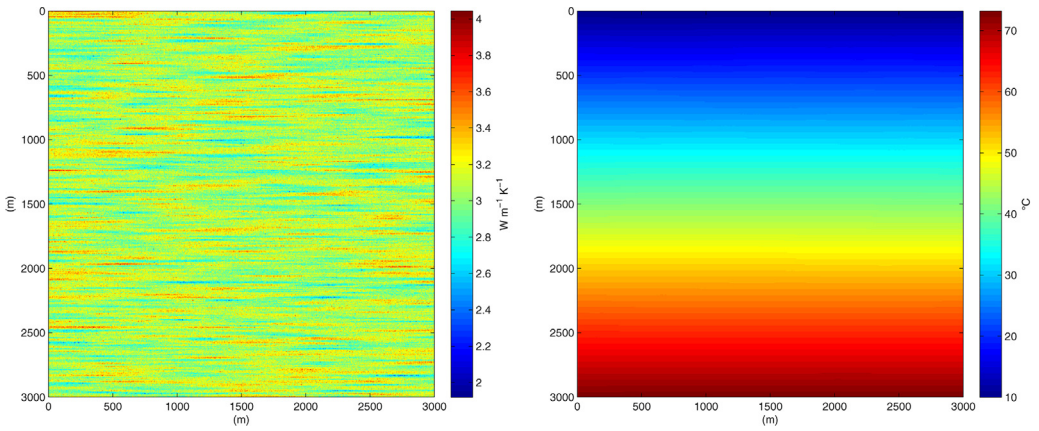

Fig. 8. Left: Random unconditional field of thermal conductivity with a 512×512 resolution. Right: Resulting temperature distribution.

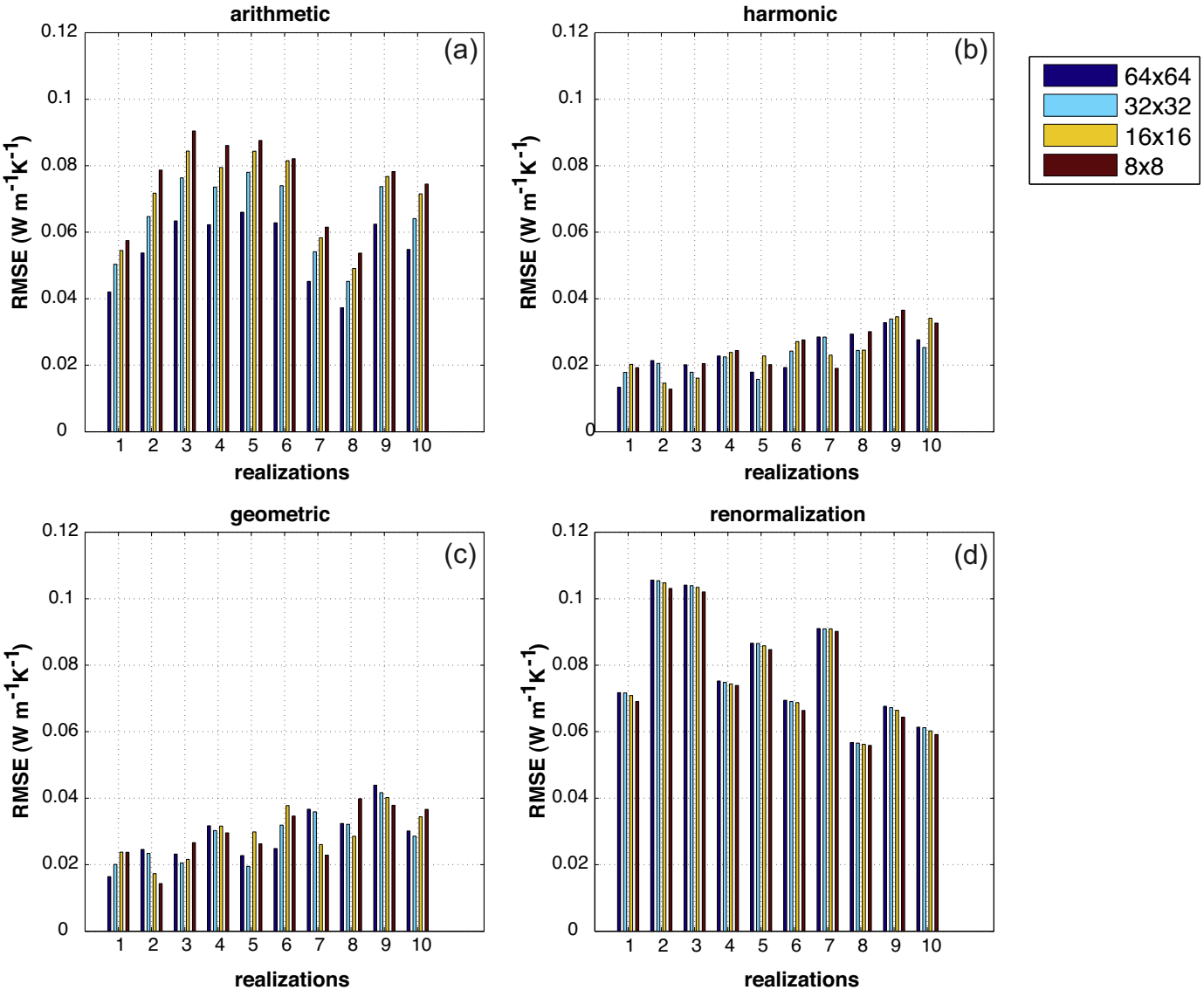

Fig. 9. Comparison of RMSE for all realizations and all scales of the arithmetic (a), harmonic (b), geometric (c) and renormalization (d) approach.

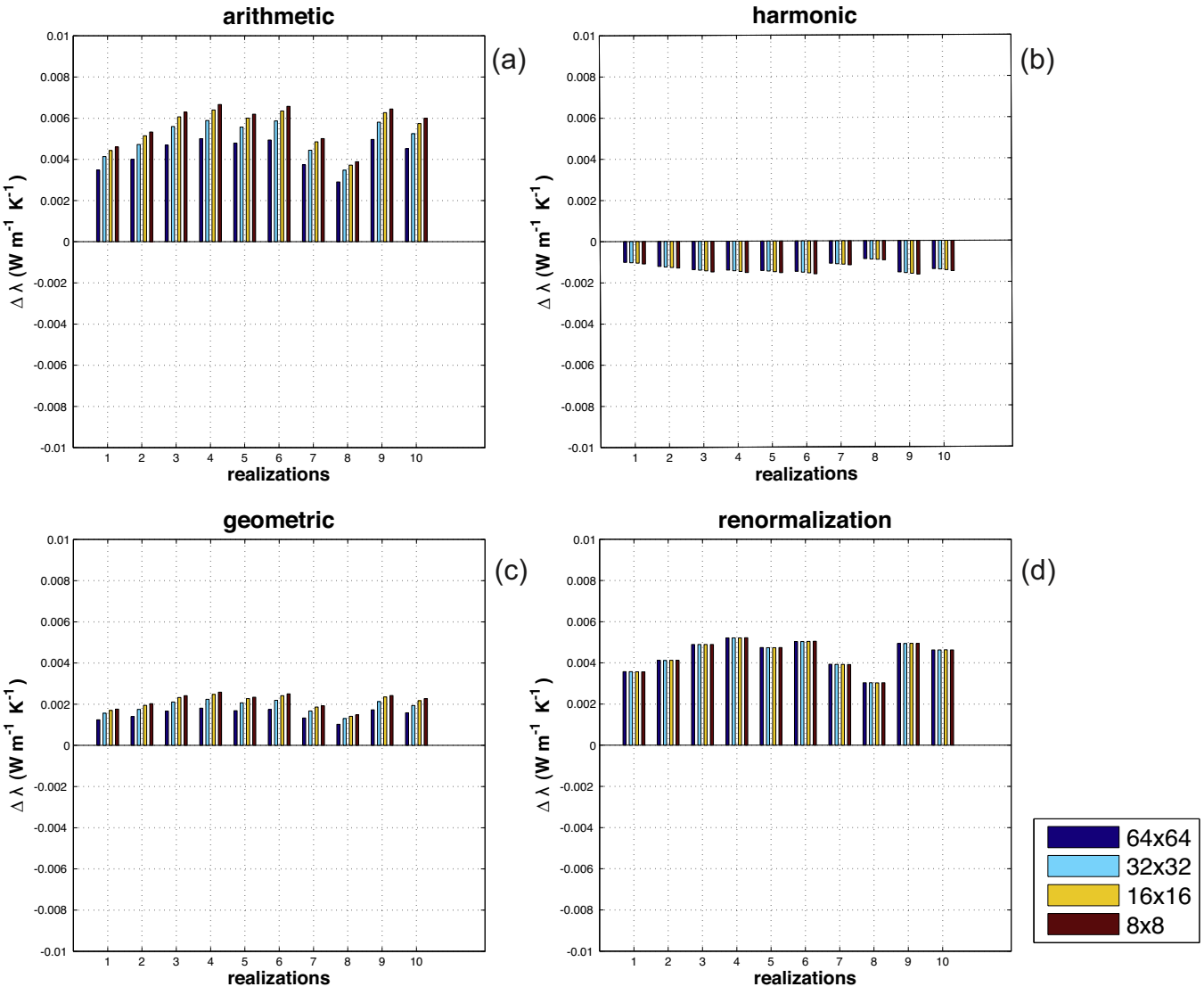

Fig. 10. Comparison for all realizations and all scales with the flow based upscaling of the arithmetic (a), harmonic (b), geometric (c) and renormalization (d) approach. The values shown are the differences of thermal conductivity compared with the result of full resolution.

3. Numerical examples of the effects of diverse upscaling techniques

3.1. Data

We study the relevance of the appropriate choice of upscaling approach through a synthetic example which is inspired to a field setting and associated data. The rock system we mimic is formed by permo-carboniferous Rotliegend clastica (Fig. 4). The basic statistics of the available thermal conductivity data originally measured along a 50 m long vertical core (80 m deep borehole GA 2 of the Messel campaign performed by the Leibniz Institute for Applied Geophysics/Hannover-Germany in 2004) are listed in Table 2. Measurements were taken in the core at intervals of approximately 1mm using a thermal conductivity scanner (designed by Lippmann and Rauen according to Popov et al., 1983, 1999).

The Messel pit (20 km south of Frankfurt, Germany), well known for its fossil-rich oil shales (Harms, 2002; Schulz et al., 2002) formed as a maar structure by phreatomagmatic explosions 47 Ma ago along a fault zone (Schulz et al., 2005; Mezger et al., 2013). It is located on the Sprendlinger Horst, a Paleozoic Horst structure east of the northern Upper Rhine Graben. Above crystalline bedrocks of the Paleozoic Variscan basement Permo-Carboniferous volcanics and sediments of the Carboniferous to Permian Rotliegend and Mid-dle Eocene sediments have been deposited. To identify the Messel Fault Zone two fully cored boreholes called GA1 and GA2 were drilled in 2004. The cores were used to measure complete thermal conductivity profiles (Gu et al., 2013).

In addition to this dataset representative of small scale variability, we consider a dataset formed by all available thermal conductivity measurements collected from a basin scale outcrop analogue study representative of the large scale. In this study sediments of the Carboniferous to Permian Rotliegend of the Saar-Nahe Basin (Germany) (Schäfer, 2011) were sampled from outcrops and shallow (max. 250 m TVD) and deep (max. 2800 m TVD) boreholes from an area spanning 150 km in W–E and 50 km in N–S direction (Aretz et al., 2013). The basic statistics of this second data-set are listed in Table 4.

Both samples are essentially normally distributed (Fig. 5) and show similar minimum, maximum, mean and median values. Data associated with the whole northern Rheingraben are less abundant than those related to the available core and appear to be associated with an increased standard deviation/variance. The frequency distribution of thermal conductivity changes with increasing domain

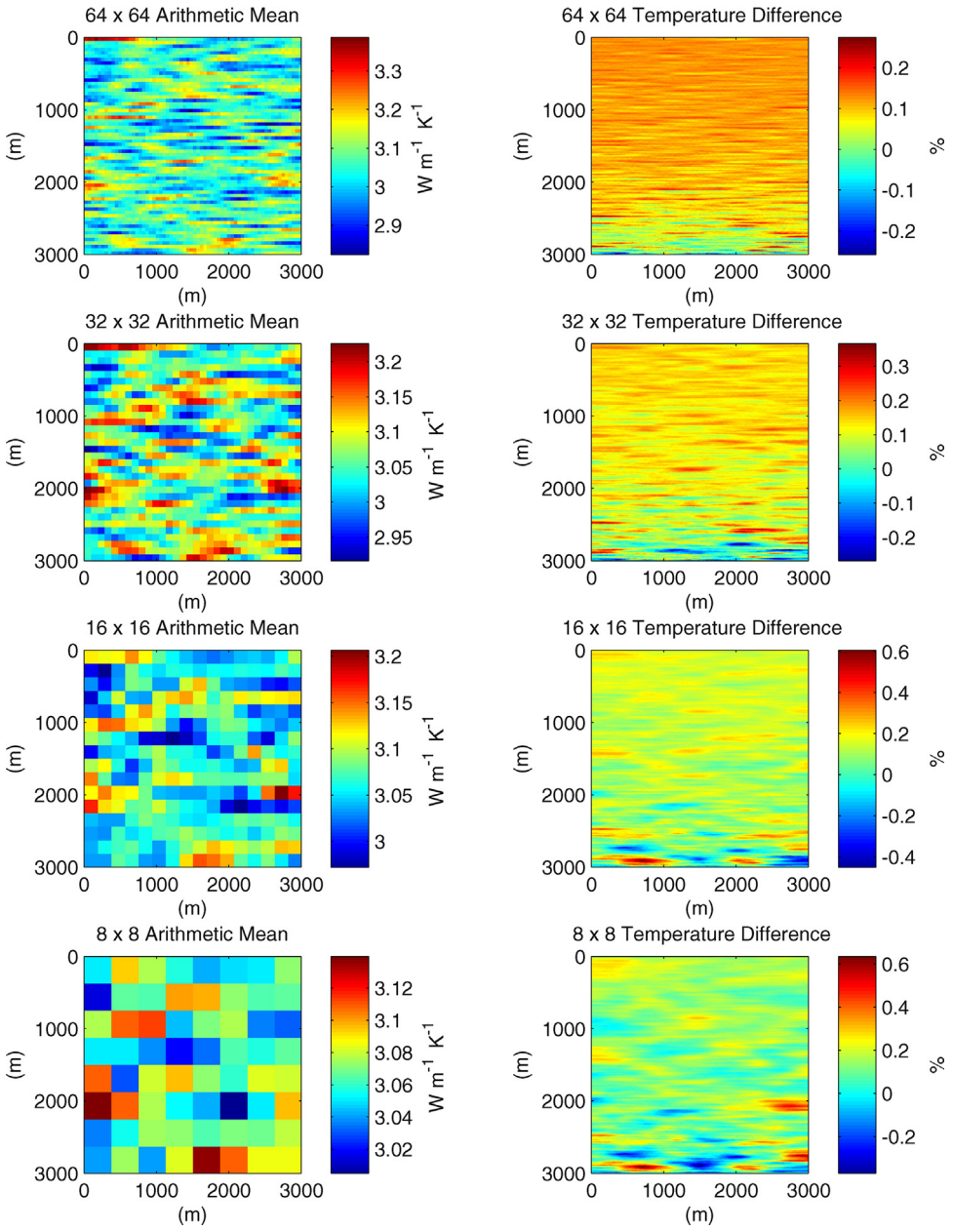

Fig. 11. Upscaled thermal conductivity distribution based on the random field shown left in Fig. 8 using 64 × 64, 32 × 32, 16 × 16 and 8 × 8 nodes, respectively. Upscaling is performed by arithmetic mean. At the right side the difference of the temperature distribution calculated this way to the original one (Fig. 8 right) is depicted in percent.

size. Even as the average value remains approximately unchanged, the variance increases considerably.

Variogram analysis has been performed on both available datasets. We consider the sample variograms associated with the borehole and outcrop data to be respectively indicative of the type of vertical and horizontal variability (in a geostatistical sense) of the spatial distribution of thermal conductivities we consider in our synthetic study. The latter is performed upon relying on a two-dimensional (along the vertical) domain, mimicking a cross-section of a sedimentary formation associated with the variogram models we derived. The vertical sample variogram could be modeled by two nested spherical structures, respectively associated with ranges of 0.4 m and 4.5 m (Fig. 6(a) and (b), Table 1). Otherwise, the horizontal sample variogram (Fig. 6(c)) could be interpreted through a spherical model associated with an estimated range of 2500 m. Table 1 lists the key results of the variogram modeling we performed.

Table 1
The three different theoretical variogram settings; all are spherical.

	Small scale	Medium scale	Large scale
Nugget	0.02	0.03	0.06
Sill	0.022	0.03	0.1
Range	0.4 m	4.5 m	2500 m

Table 2
Basic statistics of dry measured thermal conductivity ($W\,m^{-1}\,K^{-1}$) of the 50 m long core dataset.

Minimum	1.107
Maximum	3.745
Mean	2.3638
Median	2.3900
Standard deviation	0.2670
Variance	0.071
Number of observations	31,049

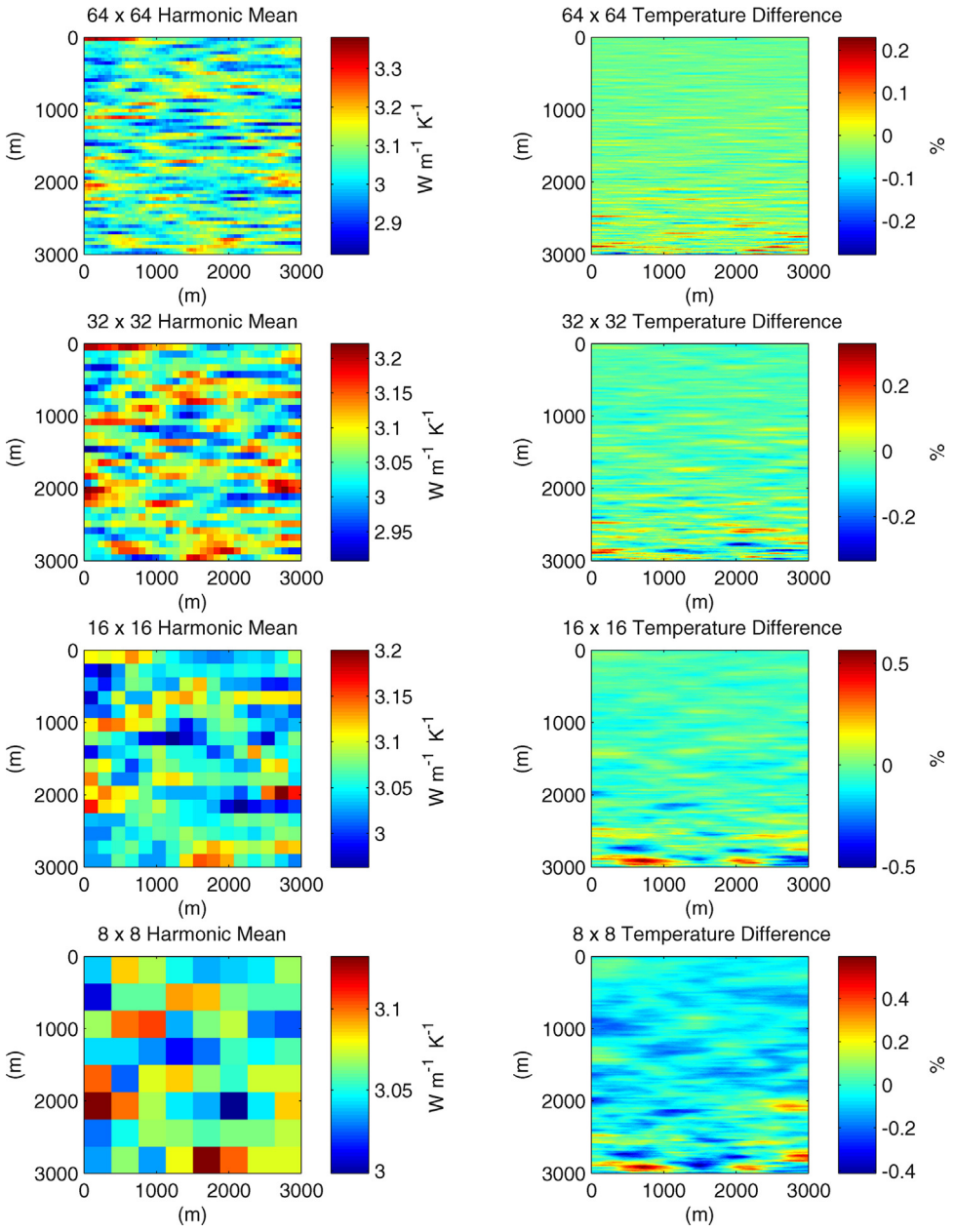

Fig. 12. Upscaled thermal conductivity distribution based on the random field shown left in Fig. 8 using 64 × 64, 32 × 32, 16 × 16 and 8 × 8 nodes, respectively. Upscaling is performed by harmonic mean. At the right side the difference of the temperature distribution calculated this way to the original one (Fig. 8 right) is depicted in percent.

Table 3
Basic statistics of water saturated measured thermal conductivity ($W\,m^{-1}\,K^{-1}$) of the 50 m long core dataset.

Minimum	1.919
Maximum	4.044
Mean	2.943
Median	2.957
Standard Deviation	0.223
Variance	0.05
Number of observations	24,079

Table 4
Basic statistics of dry measured thermal conductivity ($W\,m^{-1}\,K^{-1}$) of the large area dataset (Northern Oberrhein Graben).

Minimum	1.172
Maximum	3.59
Mean	2.3042
Median	2.3
Standard deviation	0.3874
Variance	0.150
Number of observations	611

The available data are, mainly due to technical reasons, based on measurements at dried rock samples. However, for the vertical dataset, a smaller part was also measured while saturated with water (Table 3). Details with respect to the measurements can be found in (Gu et al., 2013). Besides of a larger thermal conductivity for the water saturated values and a different, smaller sill, both range and shape of the variograms are similar from a qualitative point of view (Figs. 6 and 7). Due to a lack of saturated measurements no such correlation can be deduced for the regional dataset.

As this study aims at upscaling of reservoir thermal conductivities, data have been scaled according to the available water saturated measurements (Fig. 5(b)), while using the theoretical variograms of the dry measured dataset.

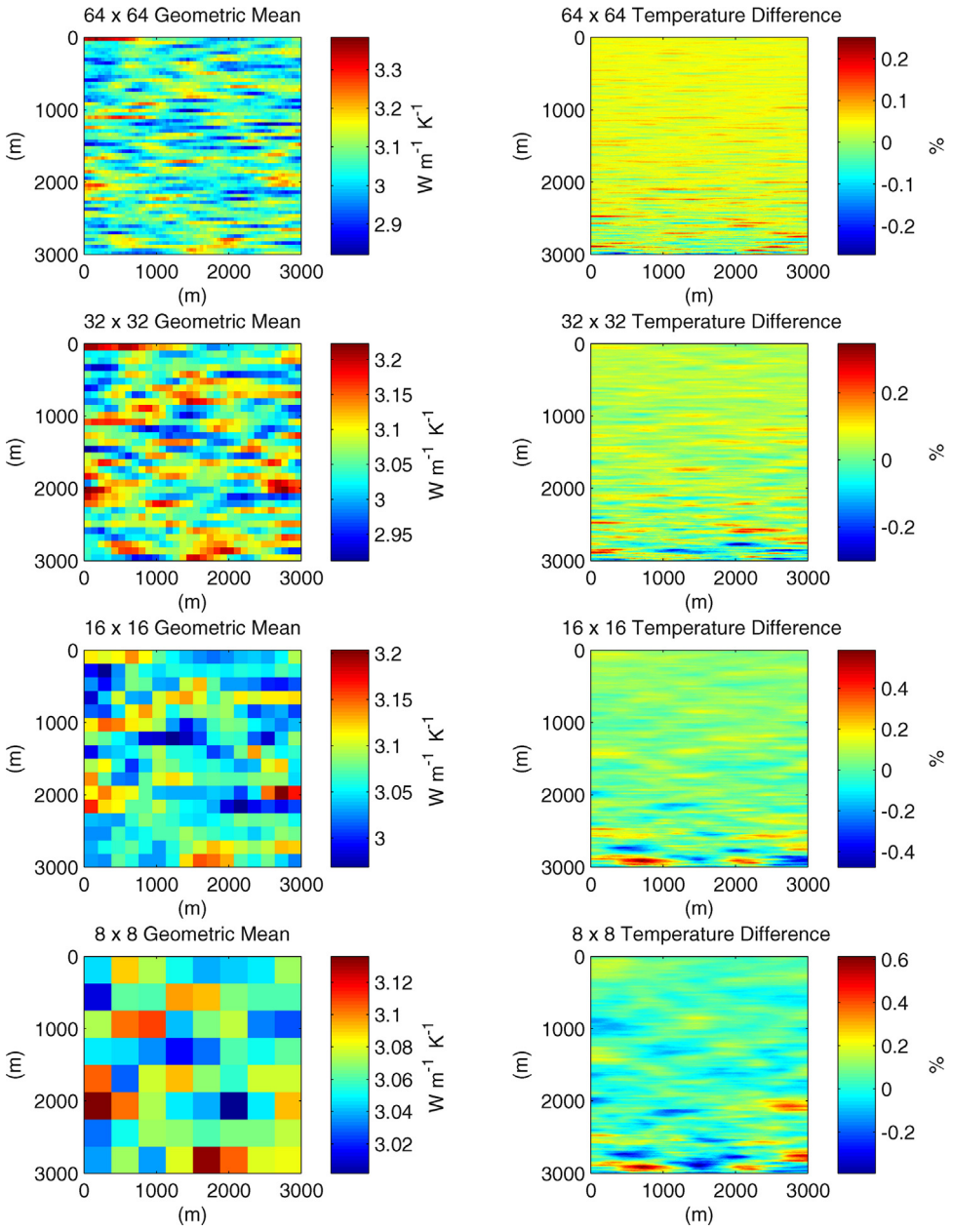

Fig. 13. Upscaled thermal conductivity distribution based on the random field shown left in Fig. 8 using 64×64, 32×32, 16×16 and 8×8 nodes, respectively. Upscaling is performed by geometric mean. At the right side the difference of the temperature distribution calculated this way to the original one (Fig. 8 right) is depicted in percent.

3.2. Methods

A discrete flow based upscaling approach (using the full dataset) is compared with the solutions we obtain upon relying on diverse power averaging exponents and renormalization.

The diverse upscaling procedures we test and the subsequent heat flow modeling (using routines based on Alberty et al., 1999) are performed in the MATLAB environment (The MathWorks, 2014).

By using all three variograms shown in Fig. 6 and Table 1, a random unconditional field of thermal conductivity on a mesh with 512×512 nodes, and a 5.86 m $\times$ 5.86 m resolution (resulting in a 3000 m $\times$ 3000 m two-dimensional vertical domain), was generated using the sequential Gaussian simulation code from the GSLIB library (Deutsch and Journel, 1998). The resulting distribution is scaled, according to water saturated conditions (Table 3), between 1.919 $\mathrm{W\,m^{-1}\,K^{-1}}$ and 4.044 $\mathrm{W\,m^{-1}\,K^{-1}}$.

Based on the random thermal conductivity distribution (Fig. 8, left), coarsened meshes with locally upscaled thermal conductivities were generated.

Four cases were considered, each of these constructed by respectively grouping 64×64, 32×32, 16×16 and 8×8 cells (see the Appendix for examples of such reconstructions).

We start by calculating upscaled thermal conductivity distributions on the basis of the original high-resolution conductivity field by using power averaging and considering diverse values of the exponent p leading to the arithmetic, harmonic, and geometric mean values, and renormalization. We then solve the steady-state conductive heat-transport equation to compute the temperature distribution for the fine-scale and upscaled conductivity fields.

3.2.1. Mathematical model and boundary conditions

Similar to MacLachlan and Moulton (2006) we consider two-dimensional (along a vertical plane) steady heat-flow through a

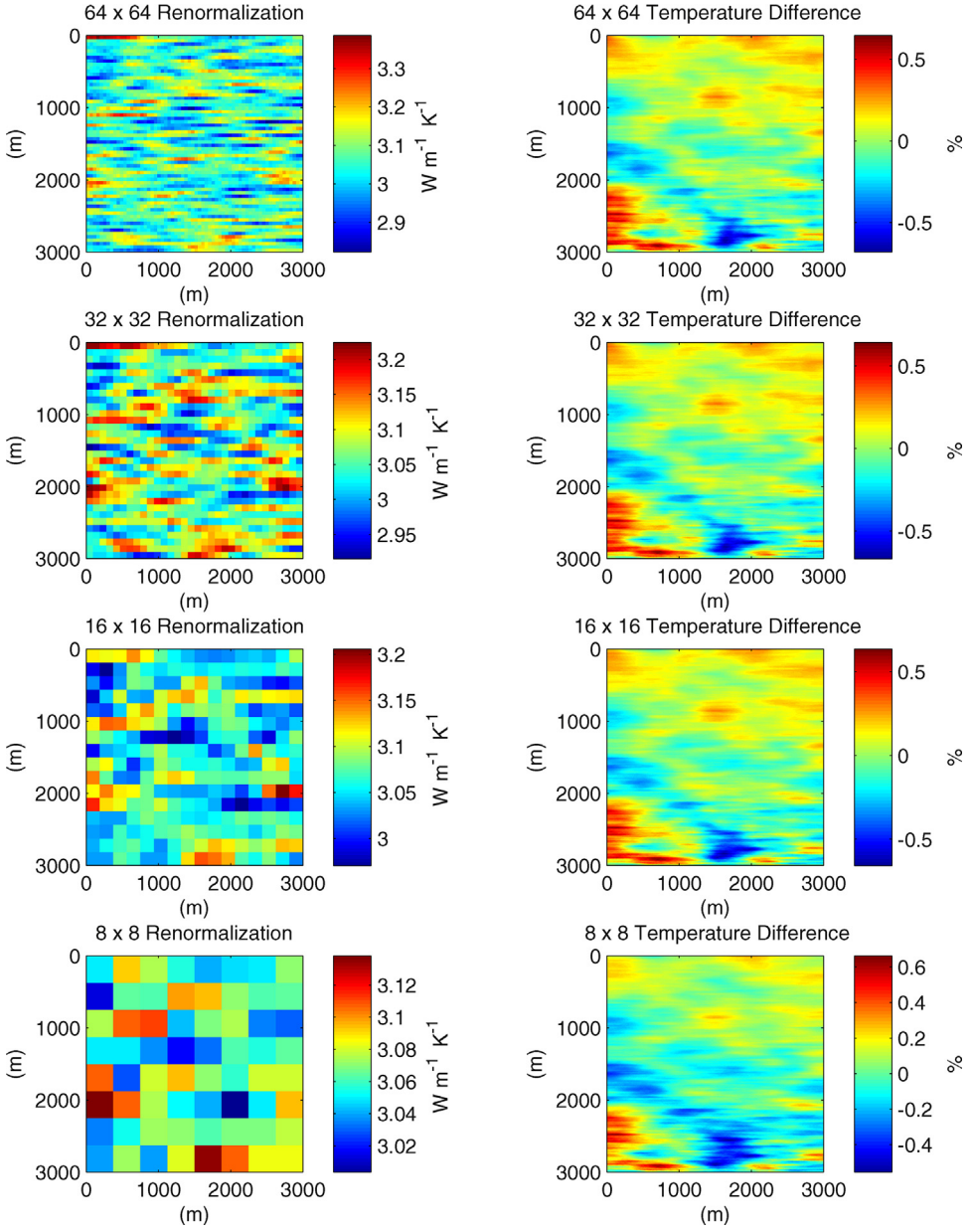

Fig. 14. Upscaled thermal conductivity distribution based on the random field shown left in Fig. 8 using 64×64, 32×32, 16×16 and 8×8 nodes, respectively. Upscaling is performed by renormalization mean. At the right side the difference of the temperature distribution calculated this way to the original one (Fig. 8 right) is depicted in percent.

rock whose thermal conductivity, $\lambda(\mathbf{x})$, is specified on a fine-scale over the domain of interest, Ω.

This flow may be modelled at the continuum scale using Fourier's law and conservation of energy (Eqs. (1) and (2)) for all $\mathbf{x} \in \Omega$, i.e.:

$$-\nabla \cdot [\boldsymbol{\lambda}(\mathbf{x}) \nabla T(\mathbf{x})] = 0. \tag{9}$$

The thermal conductivity, $\lambda(\mathbf{x})$, is a positive scalar or a positive definite tensor that is assumed to be piecewise smooth with jump discontinuities at interfaces.

We consider problems with a combination of flow boundary conditions (Neumann) and prescribed temperature (Dirichlet) at the boundaries Γ of Ω. For the bottom boundary a heat-flux of $65\,\mathrm{mW\,m^{-2}}$ is used while at the top boundary a temperature of $10\,^{\circ}\mathrm{C}$ is assigned.

Using Eq. (9) a fine-scale discrete numerical model is obtained upon relying on bilinear finite elements on a uniform rectangular mesh that resolves the variation in $\lambda(\mathbf{x})$.

3.2.2. *Numerical methods*

We employ the standard Galerkin finite element formulation to solve the heat conduction problem; for the diverse schematizations we consider.

$$T(\mathbf{x}) = \sum_{i=1}^{N} T_i \phi_i(\mathbf{x}), \tag{10}$$

where $\{\phi_i(\mathbf{x})\}$ are the nodal basis functions associated with the rectangular mesh of N nodes. Substitution of (10) into the weak form of (9) results in a discrete problem that may be expressed as a sparse linear system of equations:

$$\mathbf{A}\mathbf{b} = \mathbf{x}. \tag{11}$$

Here **b** defines the resulting temperatures which are resulting from the large, sparse $N \times N$ matrix, **A**, which elements are given by:

$$a_{ij} = \int_{\Omega} (\lambda(\mathbf{x}) \nabla \phi_i(\mathbf{x})) \cdot \nabla \phi_j(\mathbf{x}) d\Omega. \quad (12)$$

Since $\lambda(\mathbf{x})$ is symmetric and positive definite, so is **A**.

3.3. Results

For each of 10 simulated system realizations upscaling is performed (using Eqs. (3) and (8)) and the temperature results for the upscaled grid are subtracted from the results of the original distribution (Fig. 8, right). In order to avoid numerical effects due to different grid resolutions, all upscaled distributions have the same resolution (512×512) as the initial data set. As such, neighboring elements have identical (upscaled) values of conductivity according to the level of upscaling. The resulting root mean square errors (RMSE) are compared in Fig. 9.

The RMSE is smallest for harmonic and geometric power averaging, while it is largest for the arithmetic mean and the renormalization approach.

For the arithmetic approach the RMSE is always slightly increasing with decreasing number of blocks. In case of renormalization the situation is vice versa. The RMSE of each realization associated with the harmonic and geometric approach are different. Visual inspection of our result suggest that the RMSE does not correlate with the upscaling resolution.

All upscaling methods rendered distinctly different RMSE for the different realizations.

Two-dimensional temperature differences are depicted for the last (10th) realization in the appendix (Figs. 11–14).

Finally an average thermal gradient was calculated on the basis of the mean temperatures at the model base. As the heat-flow is known, the associated (uniform) average thermal conductivity can easily be calculated. The results obtained for all model resolution scales (Fig. 10) gave similar results with only very small differences, but with some distinct characteristics: harmonic and geometric mean give smallest deviation, the harmonic mean is the only one with negative differences; arithmetic mean and renormalization are comparable good, an interesting feature is that for all power averaging means differences are increasing with decreasing reso-lution, only for renormalization the differences are not related with the resolution.

4. Conclusions

Upscaling thermal conductivity can be fundamentally different from upscaling other hydrodynamic or transport parameters in porous media and rocks.

In this study a comparison of upscaling procedures for a suite of synthetic media mimicking the geostatistical structure of a sedimentary rock system has been illustrated.

The compared different upscaling approaches show only a minor impact on the resulting simulated reservoir temperatures. When upscaling is performed according to power averaging relying on a composition of local conductivities associated with their arithmetic mean, the discrepancy with the fine scale numerical solution of temperature tends to systematically increase with the degree of coarseness of the upscaled blocks. Otherwise, this discrepancy does not appear to show a clear correlation with the level of coarseness of the system description values when either harmonic or geometric mean values of local conductivities are employed in the upscaling procedure, i.e., for some realizations the error is larger for the finer grid than for the coarser one. In the case of the approach based on renormalization, the magnitude of the discrepancy is comparable for all scales tested, even as it tends to diminish for coarser levels of descriptions.

The smallest RMSE is generally associated with the harmonic and geometric mean upscaled values. The RMSEs associated with arithmetic mean upscaled values and renormalization are comparable and essentially twice the values resulting from the harmonic and geometric mean approaches.

These observations are generally consistent with findings associated with block-averaging of hydraulic conductivities in single realizations of heterogeneous two-dimensional porous media (e.g. Sánchez-Vila et al., 2006, and references therein). We note that the type of layering which is considered in this study is commonly found in sedimentary rock formations in diverse parts of the world. As such, ours can be considered an observation-driven study from which one could then develop future synthetic scenarios within which the impact of diverse principal directions of anisotropy could be systematically analyzed.

Finally, the results of the flow based upscaling reveal that the estimated amount of heat-in-place is essentially insensitive to the upscaling procedure employed.

Acknowledgements

This work is partly supported by the DFG in the framework of the Excellence Initiative, Darmstadt Graduate School of Energy Science and Engineering (GSC 1070).

A.G. acknowledges funding from MIUR (Italian Ministry of Education, Universities and Research) (PRIN2010-11 project: Innovative methods for water resources under hydro-climatic uncertainty scenarios).

S.G. thanks Foundation CMG for supporting his chair.

Appendix

In the following figures examples of the results of upscaling of the 10th and last realization of the random field (Fig. 8 left) are depicted for the four different upscaling resolutions (64×64, 32×32, 16×16 and 8×8 cells). Similar to the previous results, arithmetic, harmonic, geometric and renormalization approaches were used for the upscaling. For comparison the resulting differences between the temperature field based on the upscaled distribution and that of the original, full distribution are shown.

References

Al-Zyoud, S., Rühaak, W., Sass, I., 2014. Dynamic numerical modeling of the usage of groundwater for cooling in north east Jordan – a geothermal case study. Renew. Energy 62 (0), 63–72.

Alberty, J., Carstensen, C., Funken, S., 1999. Remarks around 50 lines of MATLAB: short finite element implementation. Numer. Algorithms 20 (2–3), 117–137.

Aretz, A., Bär, K., Sass, I., 2013. Charakterisierung des geothermischen reservoirpotenzials des permokarbons in hessen und rheinland-pfalz – thermophysikalische und hydraulische gesteinskennwerte. Swiss Bull. Angew. Geol. 18 (1), 33–41.

Bär, K., Arndt, D., Fritsche, J.-G., Götz, A.E., Kracht, M., Hoppe, A., Sass, I., 2011. 3D-Modellierung der tiefengeothermischen Potenziale von Hessen – Eingangsdaten und Potenzialausweisung. Zeitschrift der Deutschen Gesellschaft für. Geowissenschaften (ZDGG) 162 (4), 371–388, 12.

Beardsmore, G.R., Cull, J.P., 2001. Crustal Heat Flow. Cambridge University Press.

Chilès, J., Delfiner, P., 1999. Geostatistics: Modeling Spatial Uncertainty. Wiley, New York.

Christie, M., 1996. Upscaling for reservoir simulation. J. Pet. Technol. 48 (11), 1004–1010.

Christie, M., 2001. Flow in porous media – scale up of multiphase flow. Curr. Opin. Colloid Interface Sci. 6 (3), 236–241.

Chu, L., Schatzinger, R., 1996. Topical Report Application of Wavelet Analysis to Upscaling of Rock Properties for Management and Operating Contract for the Department of Energy's National Oil and Related Programs. Tech. Rep. U.S. Department of Energy Bartlesville Project Office, DE-AC22-94PC91008.

Clauser, C., 1992. Permeability of crystalline rocks. EOS Trans. Am. Geophys. Union 73 (21), 233–237 (Data Update: http://www.rwth-aachen.de/geop/Forschung/Petrophysik/rocks/perm.htm).

Clauser, C., Huenges, E., 1995. Thermal conductivity of rocks and minerals. In: Ahrens, T.J. (Ed.), In: Rock Physics and Phase Relations – A Handbook of Physical Constants, AGU Reference Shelf, vol. 3. American Geophysical Union, Washington, pp. 105–126.
Desbarats, A., 1992. Spatial averaging of hydraulic conductivity in three-dimensional heterogeneous porous media. Math. Geol. 24 (3), 249–267.
Deutsch, C.V., Journel, A.G., 1998. GSLIB: Geostatistical Software Library and Users's Guide, 2nd ed. Oxford University Press, Oxford.
Farmer, C.L., 2002. Upscaling: a review. Int. J. Numer. Methods Fluids 40 (1–2), 63–78.
Förster, A., Merriam, D.F. (Eds.), 1999. Geothermics in Basin Analysis. Kluwer, New York.
Fuchs, S., Förster, A., 2010. Rock thermal conductivity of Mesozoic geothermal aquifers in the Northeast German Basin. Chem. Erde Geochem. 70 (Supplement 3 (0)), 13–22 (Geoenergy: From Visions to Solutions).
Goovaerts, P., 1997. Geostatistics for Natural Resources Evaluation. Oxford University Press, New York, USA.
Green, C., Paterson, L., 2007. Analytical three-dimensional renormalization for calculating effective permeabilities. Transp. Porous Media 68 (2), 237–248. Gu, Y., Rühaak, W., Bär, K., Sass, I., 2013. Joint Kriging of geothermal reservoir properties – methods and challenges. In: Proceedings of the European Geothermal Congress 2013, Pisa, Italy.
Guadagnini, A., Neuman, S., Nan, T., Riva, M., Winter, C., 2015. Scalable statistics of correlated random variables and extremes applied to deep borehole porosities. Hydrol. Earth Syst. Sci. 19, 729–745.
Guadagnini, A., Neuman, S., Schaap, M., Riva, M., 2013. Anisotropic statistical scaling of vadose zone hydraulic property estimates near Maricopa, Arizona. Water Resour. Res. 49, 1–17.
Haenel, R., Staroste, E., 1988. Atlas of Geothermal Resources in the European Community, Austria, and Switzerland. EUR (Series). Directorate-General for Science, Research and Development, Geothermal Research, Brussels.
Harms, F.-J., 2002. On the origin of the Messel Pit and other oil shale deposits on the Sprendlinger Horst, Southern Hessen. Terra Nostr. 6, 160–164.
Hartmann, A., Rath, V., Clauser, C., 2005. Thermal conductivity from core and well log data. Int. J. Rock Mech. Min. Sci. 42, 1042–1055.
Hastings, J., Muggeridge, A., 2001. Upscaling uncertain permeability using small cell renormalization. Math. Geol. 33 (4), 491–505.
Hayba, D.O., Ingebritsen, S.E., 1997. Multiphase groundwater flow near cooling plutons. J. Geophys. Res.: Solid Earth 102 (B6), 12235–12252, http://dx.doi.org/10.1029/97JB00552.
Homuth, S., Götz, A.E., Sass, I., 2014. Lithofacies and depth dependency of thermo- and petrophysical rock parameters of the Upper Jurassic geothermal carbonate reservoirs of the Molasse Basin. Z. Dt. Ges. Geowiss. 165 (3), 469–486.
Huenges, E., Kohl, T., Kolditz, O., Bremer, J., Scheck-Wenderoth, M., Vienken, T., 2013. Geothermal energy systems: research perspective for domestic energy provision. Environ. Earth Sci. 70 (8), 3927–3933.
Journel, A.G., Deutsch, C.V., Desbarats, A.J., 1986. Power averaging for block effective permeability. In: Paper SPE 15128 Presented at the SPE California Regional Meeting, April 2–4, 1986, Oakland, New York.
Karim, M., Krabbenhoft, K., 2010. New renormalization schemes for conductivity upscaling in heterogeneous media. Transp. Porous Media 85 (3), 677–690.
King, P., 1989. The use of renormalization for calculating effective permeability. Transp. Porous Media 4 (1), 37–58.
Li, L., Zhou, H., Hendricks Franssen, H.-J., Gomez-Hernandez, J.J., 2012. Modeling transient groundwater flow by coupling ensemble Kalman filtering and upscaling. Water Resour. Res. 48 (1).
Lu, P., 2001. Reservoir Parameter Estimation Using Wavelet Analysis (Ph.D. thesis). Stanford University, Dept. of Petroleum Engineering.
Lunati, I., Bernard, D., Giudici, M., Parravicini, G., Ponzini, G., 2001. A numerical comparison between two upscaling techniques: non-local inverse based scaling and simplified renormalization. Adv. Water Resour. 24 (8), 913–929.
MacLachlan, S.P., Moulton, J.D., 2006. Multilevel upscaling through variational coarsening. Water Resour. Res. 42 (2).
Mezger, J., Felder, M., Harms, F.-J., 2013. Crystalline rocks in the maar deposits of messel: key to understand the geometries of the messel fault zone and diatreme and the post-eruptional development of the basin fill. Z. Dtsch. Ges. Geowiss. 164, 639–662.
Neuman, S., Guadagnini, A., Riva, M., Siena, M., 2013. Recent advances in statistical and scaling analysis of earth and environmental variables. In: Mishra, P., Kuhlman, K. (Eds.), Advances in Hydrogeology. Springer Science+Business Media, New York, pp. 11–15.
Nield, D.A., Bejan, A., 1999. Convection in Porous Media. Springer, New York.
Popov, Y.A., Sass, P.D., Williams, J., Burkhardt, C.H., 1999. Characterization of rock thermal conductivity by high resolution optical scanning. Geothermics 28 (2), 253–276.
Popov, Y., Semionov, V., Korosteliov, V., Berezin, V., 1983. Non-contact evaluation of thermal conductivity of rocks with the aid of a mobile heat source. Izv. Phys. Solid Earth 19, 563–567.
Press, W.H., Teukolsky, S.A., Vetterling, W.T., Flannery, B.P., 1992. Numerical Recipes in C (2nd ed.): The Art of Scientific Computing. Cambridge University Press, New York, NY, USA.
Pribnow, D., Umsonst, T., 1993. Estimation of thermal conductivity from the mineral composition: influence of fabric and anisotropy. Geophys. Res. Lett. 20 (20), 2199–2202.
Pyrcz, M.J., Deutsch, C.V., 2014. Geostatistical Reservoir Modeling, second ed. Oxford University Press, New York, USA.
Rath, V., Wolf, A., Bücker, H.M., 2006. Joint three-dimensional inversion of coupled groundwater flow and heat transfer based on automatic differentiation: sensitivity calculation, verification, and synthetic examples. Geophys. J. Int. 167 (1), 453–466.
Renard, P., de Marsily, G., 1997. Calculating equivalent permeability: a review. Adv. Water Resour. 20 (5–6), 253–278.
Reza Rasaei, M., Sahimi, M., 2008. Upscaling and simulation of waterflooding in heterogeneous reservoirs using wavelet transformations: application to the SPE-10 model. Transp. Porous Media 72 (3), 311–338.
Riva, M., Neuman, S., Guadagnini, A., 2013. Sub-Gaussian model of processes with heavy tailed distributions applied to permeabilities of fractured tuff. Stoch. Environ. Res. Risk Assess. 27, 195–207.
Rühaak, W., Rath, V., Clauser, C., 2010. Detecting thermal anomalies within the Molasse Basin, southern Germany. Hydrogeol. J. 18 (8), 1897–1915.
Sánchez-Vila, X., Guadagnini, A., Carrera, J., 2006. Representative hydraulic conductivities in saturated groundwater flow. Rev. Geophys. 44 (RG3002).
Sass, I., Götz, A.E., 2012. Geothermal reservoir characterization: a thermofacies concept. Terra Nova 24 (2), 142–147.
Sass, J.H., Lachenbruch, A.H., Munroe, R.J., 1971. Thermal conductivity of rocks from measurements on fragments and its application to heat-flow determinations. J. Geophys. Res. 76 (14), 3391–3401.
Schäfer, A., 2011. Tectonics and sedimentation in the continental strike-slip saar-nahe basin (carboniferous-permian, west germany). Z. dt. Ges. Geowiss. 162 (2), 127–155.
Scheibe, T., Yabusaki, S., 1998. Scaling of flow and transport behavior in heterogeneous groundwater systems. Adv. Water Resour. 22 (3), 223–238.
Schulz, R., Buness, H., Gabriel, G., Pucher, R., Rolf, C., Wiederhold, H., Wonik, T., 2005. Detailed investigation of preserved maar structures by combined geophysical surveys. Bull. Volcanol. 68, 95–106.
Schulz, R., Harms, F.-J., Felder, M., 2002. Die forschungsbohrung messel 2001. Ein beitrag zur entschlüsselung der genese einer ölschieferlagerstätte. Z. Angew. Geol. 4, 9–17.
Sippel, J., Fuchs, S., Cacace, M., Braatz, A., Kastner, O., Huenges, E., Scheck-Wenderoth, M., 2013. Deep 3D thermal modelling for the city of Berlin (Germany). Environ. Earth Sci., 1–22.
Sundberg, J., Back, P.-E., Ericsson, L.O., Wrafter, J., 2009. Estimation of thermal conductivity and its spatial variability in igneous rocks from in situ density logging. Int. J. Rock Mech. Min. Sci. 46 (6), 1023–1028.
The MathWorks, I., 2014. Matlab 2014. Natick, Massachusetts.
Tukey, J., 1977. Exploratory Data Analysis, 1st ed. Reading (Addison-Wesley).
Vogt, C., Mottaghy, D., Wolf, A., Rath, V., Pechnig, R., Clauser, C., 2010. Reducing temperature uncertainties by stochastic geothermal reservoir modelling. Geophys. J. Int. 181 (1), 321–333.
Wen, X.-H., Gomez-Hernandez, J., 1996. Upscaling hydraulic conductivities in heterogeneous media: an overview. J. Hydrol. 183 (1–2), ix–xxxii.
Williams, C.F., Anderson, R.N., 1990. Thermophysical properties of the earth's crust: in situ measurements from continental and ocean drilling. J. Geophys. Res.: Solid Earth 95 (B6), 9209–9236.
Zhang, S., Klimentidis, R.E., Barthelemy, P., 2012. From micron to millimeter upscaling of shale rock properties based on 3D imaging and modeling. In: International Symposium of the Society of Core Analysts, Aberdeen, Scotland, UK, 27–30 August, 2012, Aberdeen, Scotland, UK, 27–30 August, 2012. Society of Core Analysts, Scotland, pp. 27–30.